Kinetic broadening of size distribution in terms of natural versus invariant variables

Vladimir G. Dubrovskii,[1,*] Nickolay V. Sibirev,[1] and Andrei S. Sokolovskii[2]
[1]*St. Petersburg State University, Universitetskaya Embankment 13B, 199034 St. Petersburg, Russia*
[2]*ITMO University, Kronverkskiy Prospect 49, 197101 St. Petersburg, Russia*

(Received 1 September 2020; revised 28 November 2020; accepted 23 December 2020; published 13 January 2021)

We study theoretically the size distributions of nanoparticles (islands, droplets, nanowires) whose time evolution obeys the kinetic rate equations with size-dependent condensation and evaporation rates. Different effects are studied which contribute to the size distribution broadening, including kinetic fluctuations, evaporation, nucleation delay, and size-dependent growth rates. Under rather general assumptions, an analytic form of the size distribution is obtained in terms of the natural variable s which equals the number of monomers in the nanoparticle. Green's function of the continuum rate equation is shown to be Gaussian, with the size-dependent variance. We consider particular examples of the size distributions in either linear growth systems (at a constant supersaturation) or classical nucleation theory with pumping (at a time-dependent supersaturation) and compare the spectrum broadening in terms of s versus the invariant variable ρ for which the regular growth rate is size independent. For the growth rate scaling with s as s^α (with the growth index α between 0 and 1), the size distribution broadens for larger α in terms of s, while it narrows with α if presented in terms of ρ. We establish the conditions for obtaining a time-invariant size distribution over a given variable for different growth laws. This result applies for a wide range of systems and shows how the growth method can be optimized to narrow the size distribution over a required variable, for example, the volume, surface area, radius or length of a nanoparticle. An analysis of some concrete growth systems is presented from the viewpoint of the obtained results.

DOI: 10.1103/PhysRevE.103.012112

I. INTRODUCTION

The rate equation (RE) approach is widely used for understanding and modeling the time evolution of the size distributions (SDs) of different nanoparticles including surface islands, droplets, clusters, molecular chains, and semiconductor nanowires (NWs) in different environments [1–30]. It is common to compare the measured SDs to the Poisson distribution whose variance σ^2 equals the mean size $\langle s\rangle$ [31]. In the specific case of vertical semiconductor NWs grown by the vapor-liquid-solid method [31–38], we are interested in the SD $f(s,\tau)$ over the dimensionless length s (measured in the number of monolayers) which depends on the dimensionless time $\tau = t/t_g$, where t_g is the time required to deposit one monolayer of material from vapor. If semiconductor monolayers are added randomly and independently of the nanowire length, the Poisson SD is observed with the variance $\sigma^2 = \langle s\rangle = \tau$. Without one specific effect of nucleation antibunching originating from a limited amount of material available for growth from a nanosized droplet [36–39], the Poisson SD is the best case regarding the nanowire length uniformity. Poissonian broadening of the SD originates from kinetic fluctuations described by the second derivative with respect to size in the continuum Fokker-Planck RE [8,21,31,32,37]. Other effects such as a nucleation delay for NWs emerging from a substrate [31,32,37], surface diffusion of adatoms from the nanowire sidewalls (yielding the nanowire growth rate $ds/d\tau \propto s$ for large enough s) [33,34], and desorption of material from the catalyst droplet [35] contribute to the SD spreading larger than Poissonian. The asymptotically widest Polya (or gamma) SD with $\sigma^2 \propto \langle s\rangle^2$ is observed for NWs growing by surface diffusion of adatoms [33]. Interestingly, the Polya SD and its more complex modification accounting for the nucleation delay [34] obeys the Vicsek-Family scaling property [13] which has been widely discussed in connection with epitaxial surface islands [3,6,7,16]. For a variety of growth systems, including droplets [5] and aerosols [19] in vapors, surface islands [2,4,8], Stranski-Krastanov quantum dots [17,18,24,26], and NWs [32–38,40,41], it is highly desirable to achieve the narrowest possible SD in terms of a given variable.

Recently, we have presented an analytic form of the continuum SD in linear growth systems at a constant supersaturation of a mother phase (such as vapor for vapor-liquid-solid NWs) and without [31]. Here, we generalize this approach to include systems with evaporation and time-dependent supersaturation. In the case of open systems with pumping, the large time asymptotic behavior of supersaturation is determined by the growth law and the time dependence of the material influx [21]. We obtain an analytic form of the SD in terms of the natural variables s and τ. For the growth law of the form $ds/d\tau \propto s^\alpha$ at large enough s, with the growth index α ranging from 0 to 1, Green's function of the continuum RE is shown to be Gaussian, with the mean size and variance being critically dependent on the growth index α and the evaporation rate. The SDs are additionally broadened by the nucleation delay. We consider two systems, with either constant or time-dependent

*dubrovskii@mail.ioffe.ru

supersaturation ζ, with an emphasis put on the SD broadening caused by different effects. The resulting analytic SDs over the natural variable are then compared to those rewritten in terms of the so-called invariant size variable for which the regular growth rate is size independent [$dr/d\tau = 1$ in linear growth or $d\rho/d\tau = \zeta(\tau)$ in systems with a time-dependent supersaturation ζ]. Such a variable was introduced earlier in classical nucleation theory (CNT) by Kuni *et al.* in Refs. [5,12,14], where it was argued that the SD over this variable is not affected by kinetic fluctuations. By comparing the SDs in terms of the natural versus invariant variables, we find that the broadening trends are directly opposite. In particular, the natural SD broadens with increasing α, while the invariant SD narrows with increasing α, with the Poisson SD resumed for both variables only at $\alpha = 0$. Therefore, the choice of a size-dependent variable is very important for theoretical analysis as well as practical use of the SDs. Furthermore, we establish the conditions for obtaining a time-invariant size distribution over a given variable for different growth laws. For example, one can finely tune the growth conditions to achieve the SD narrowing for a required parameter such as the total number of monomers in the nanoparticle, its surface area, radius, or length.

II. GENERAL METHOD

We consider reaction chains $A_s + A_1 \leftrightarrow A_{s+1}$ or $A_sB + A_1 \leftrightarrow A_{s+1}B$ for homogeneous or heterogeneous growth, respectively, where A_s is a homogeneous nanoparticle containing s monomers, A_sB is a heterogeneous nanoparticle containing s monomers and one foreign nucleus B, both growing by attaching (condensation) and losing (evaporation) free monomers A_1. The condensation and evaporation rate constants are denoted W_s^+ and W_{s+1}^-, respectively. They depend on s and may depend on time. The set of REs for the discrete SD $f_s(\tau)$ writes [1,2,4–12]

$$\frac{df_s(\tau)}{d\tau} = W_{s-1}^+ f_{s-1}(\tau) + W_{s+1}^- f_{s+1}(\tau) - [W_s^+ + W_s^-] f_s(\tau), \tag{1}$$

with $\tau = t/t_g$ as the dimensionless time in the units of the characteristic growth time t_g. For large enough s, this is reduced to one Fokker-Planck RE for the continuum SD $f(s,\tau)$,

$$\frac{\partial f(s,\tau)}{\partial \tau} = -\frac{\partial}{\partial s}\{[W^+(s) - W^-(s)] f(s,\tau)\} + \frac{1}{2}\frac{\partial^2}{\partial s^2}\{[W^+(s) + W^-(s)] f(s,\tau)\}, \tag{2}$$

which is the central object in what follows. Here, the variable s becomes continuum.

Assuming for the moment the time-independent rate constants (the time dependence will be included later), we introduce the invariant size by the general definition [12,21,22]

$$r = \int_0^s \frac{ds'}{W^+(s') - W^-(s')}, \tag{3}$$

which is reduced to the one in Ref. [31] in the absence of evaporation [$W^-(s) = 0$]. The new SD over r is given by

$$g(r,\tau) = [W^+(s) - W^-(s)]\, f(s,\tau). \tag{4}$$

From $ds/d\tau = W^+(s) - W^-(s)$, we obtain $dr/d\tau = 1$, the size-independent regular growth rate for r, which explains the term "invariant variable." Using this SD, Eqs. (2)–(4) yield the new RE of the form

$$\frac{\partial g(r,\tau)}{\partial \tau} = -\frac{\partial}{\partial r}\left\{ g(r,\tau) - \frac{1}{2}\frac{1}{W^+(r) - W^-(r)}\frac{\partial}{\partial r}\left[\frac{W^+(r) + W^-(r)}{W^+(r) - W^-(r)} g(r,\tau)\right]\right\}. \tag{5}$$

In what follows, we assume that

$$\frac{\partial}{\partial r}\left[\frac{1}{W^+(r) - W^-(r)}\right] \ll 1, \tag{6}$$

which is the usual case [31]. Then Eq. (5) simplifies to

$$\frac{\partial g(r,\tau)}{\partial \tau} = -\frac{\partial g}{\partial r} + \frac{1}{2}\frac{\partial^2}{\partial r^2}\left[\frac{1}{y(r)} g(r,\tau)\right], \tag{7}$$

with

$$y(r) = \frac{[W^+(r) - W^-(r)]^2}{W^+(r) + W^-(r)}. \tag{8}$$

Here, the condensation-evaporation rate constants should be expressed in terms of r using Eq. (3). Clearly, $y(r) = W^+(r)$ at $W^- = 0$, the case considered earlier in Ref. [31]. According to Refs. [21,22], if the variance of the SD increases with time slower than the mean size squared, we can further simplify the continuum RE using $y(r) \cong y(\tau)$ with high accuracy. For the RE

$$\frac{\partial g(r,\tau)}{\partial \tau} = -\frac{\partial g}{\partial r} + \frac{1}{2y(\tau)}\frac{\partial^2 g(r,\tau)}{\partial r^2}, \tag{9}$$

the exact Green function is given by the Gaussian [21]

$$G(r,\tau) = \frac{1}{\sqrt{2\pi\psi(\tau)}} \exp\left[-\frac{(r-\tau)^2}{2\psi(\tau)}\right] \tag{10}$$

with the mean invariant size τ. The variance of this Green function is obtained by solving the equation

$$\frac{d\psi}{d\tau} = \frac{1}{y(\tau)}, \quad \psi(\tau = 0) = 0, \tag{11}$$

where y is defined in Eq. (8).

To return to the natural size, we introduce the mean natural size of Green's function according to [31]

$$\frac{d\bar{s}}{d\tau} = W^+(\bar{s}) - W^-(\bar{s}), \quad \bar{s}(\tau = 0) = 0. \tag{12}$$

Using $d\psi/d\tau = (d\psi/d\bar{s})(d\bar{s}/d\tau)$, Eq. (11) for the variance takes the form

$$\frac{d\psi}{d\bar{s}} = \frac{W^+(\bar{s}) + W^-(\bar{s})}{[W^+(\bar{s}) - W^-(\bar{s})]^3}, \quad \psi(\bar{s} = 0) = 0. \tag{13}$$

Integration gives

$$\psi(\bar{s}) = \int_0^{\bar{s}} ds \frac{W^+(s) + W^-(s)}{[W^+(s) - W^-(s)]^3}. \tag{14}$$

From

$$\tau = \int_0^{\bar{s}} \frac{ds}{W^+(s) - W^-(s)} \tag{15}$$

and Eq. (3) we get

$$r - \tau = \int_{\bar{s}}^{s} \frac{ds'}{W^+(s') - W^-(s')} \cong \frac{s - \bar{s}}{W^+(\bar{s}) - W^-(\bar{s})}. \tag{16}$$

The approximate expression again holds for the SDs whose variance increases much slower than the mean size squared and was checked for validity by numerical tests in Ref. [31] without evaporation. In the presence of evaporation, the corresponding results will be given in Sec. III. From Eq. (4), Green's function in terms of the natural variable s is obtained by

$$F(s, \bar{s}) = \frac{G(s, \bar{s})}{W^+(s) - W^-(s)}. \tag{17}$$

Using Eqs. (10), (16), and (17), our general result for Green's function becomes

$$F(s, \bar{s}) = \frac{1}{\sqrt{2\pi D(\bar{s})}} \exp\left[-\frac{(s - \bar{s})^2}{2D(\bar{s})}\right]. \tag{18}$$

Here, the variance of Green's function in terms of the natural variables is given by

$$D(\bar{s}) = [W^+(\bar{s}) - W^-(\bar{s})]^2 \int_0^{\bar{s}} ds \frac{W^+(\bar{s}) + W^-(\bar{s})}{[W^+(\bar{s}) - W^-(\bar{s})]^3}. \tag{19}$$

This is reduced to $D(\bar{s}) = [W^+(\bar{s})]^2 \int_0^{\bar{s}} ds/[W^+(s)]^2$ at $W^- = 0$, which is the result of Ref. [31] in the absence of evaporation.

Thus, the general recipe for obtaining the analytic SD for a concrete growth system [characterized entirely by the size-dependent rate constants $W^{\pm}(s)$] is the following. Green's function is the Gaussian given by Eq. (18). The mean size of Green's function depends on time as given by Eq. (15), which should be inverted for a given rate constant to yield explicitly $\bar{s}(\tau)$. The variance of Green's function depends on the mean size as given by Eq. (19). Its integration gives explicitly $D(\bar{s})$ or $D(\tau)$. This completes the determination of Green's function. The real SD is then obtained by convolution of this Green function with a time-dependent nucleation rate [22,31,32,37]. In heterogeneous nucleation such as nucleation of vapor-liquid-solid NWs on a dissimilar substrate, the nucleation rate is often given by exponential decay [31,37], while in homogeneous nucleation with a time-dependent supersaturation under a material influx it is double exponential [14,18,22,42]. Some examples will be considered in the next sections. It is clear however that even if the nucleation stage is long, it can only add a constant variance to the one present in Green's function. It will be shown below that $D(\bar{s})$ increases with $\bar{s}$ for most systems (excluding the one influenced by nucleation antibunching [37]) and hence tends to infinity at $\bar{s} \to \infty$. Therefore, the asymptotic broadening of the SD in the large time limit is determined entirely by Green's function, while the influence of the nucleation-induced broadening can be significant only for small enough particles.

III. LINEAR GROWTH SYSTEMS

The regular growth rate of NWs growing by surface diffusion is given by

$$\frac{dL}{dt} = V\left(1 + \frac{2L}{R}\right)(1 - \beta) \quad \text{if } L < \Lambda,$$
$$\frac{dL}{dt} = V\left(1 + \frac{2\Lambda}{R}\right)(1 - \beta) \quad \text{if } L \geqslant \Lambda. \tag{20}$$

Here, L is the nanowire length and R is its radius, V is the effective deposition rate in nm/s, Λ is the effective diffusion length of sidewall adatoms [33,34,43,44], and β is the fraction of atoms evaporated from the droplet or transferred from the droplet to the nanowire sidewalls by downward diffusion [43,44]. Of course, NWs can grow only when $\beta < 1$. Equations (20) show that the axial growth rate is a linear function of L for short enough NWs with $L < \Lambda$ which collect adatoms from their entire length, while it becomes independent of length for longer NWs with $L \geqslant \Lambda$. The deposition rate V is time independent, corresponding to a constant supersaturation of vapor with respect to the solid state. Introducing $s = L/h$, which equals the number of monolayers of height h in a nanowire, Eq. (20) for short NWs can be put as

$$\frac{ds}{d\tau} = (1 + \gamma s)(1 - \beta),$$

with an obvious definition for γ. It is easy to see that $\gamma \ll 1$ in the typical cases, which justifies the assumption of the variance being much smaller than the mean size squared. This is an example of the linear growth system at a constant supersaturation of vapor in which the regular growth rate is a linear function of s and becomes proportional to s for large enough s.

We now consider a more general model,

$$\frac{ds}{d\tau} = (1 + \gamma s)^{\alpha}(1 - \beta), \quad 0 \leqslant \alpha \leqslant 1, \tag{21}$$

where α is the growth index determined by the material transport mechanism [21,31], $\gamma \ll 1$ determines the strength of surface diffusion relative to the direct influx, and β remains as the relative evaporation rate. For this model, we have $W^+(s) - W^-(s) = (1 + \gamma s)^{\alpha}(1 - \beta)$ and $W^+(s) + W^-(s) = (1 + \gamma s)^{\alpha}(1 + \beta)$. Integrating Eqs. (3) and (15), we obtain

$$r = \frac{1}{\gamma(1 - \beta)(1 - \alpha)}[(1 + \gamma s)^{1-\alpha} - 1],$$
$$\tau = \frac{1}{\gamma(1 - \beta)(1 - \alpha)}[(1 + \gamma \bar{s})^{1-\alpha} - 1]. \tag{22}$$

We can infer $s(r)$ and $\bar{s}(\tau)$ as follows:

$$s = \frac{1}{\gamma}\{[1 + \gamma(1 - \beta)(1 - \alpha)r]^{1/(1-\alpha)} - 1\},$$
$$\bar{s} = \frac{1}{\gamma}\{[1 + \gamma(1 - \beta)(1 - \alpha)\tau]^{1/(1-\alpha)} - 1\}. \tag{23}$$

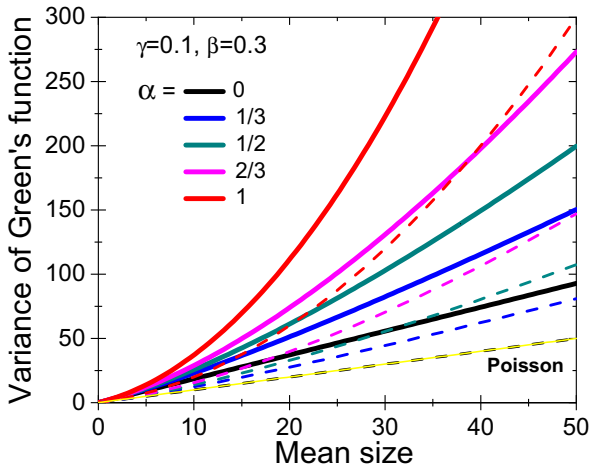

FIG. 1. Variance vs mean size of Green's function obtained from Eqs. (26) and (27) at $\gamma = 0.1$, $\beta = 0.3$ and different α shown in the legend (full lines), compared to the came systems without evaporation (dashed lines). The variance increases with the growth index α and with the evaporation coefficient β. Yellow line shows the Poisson variance which correspond to the minimum broadening of the SD and is observed at $\alpha = \beta = 0$.

For $\alpha = 1$, this converges to

$$s = \frac{1}{\gamma}\left(e^{\gamma(1-\beta)r} - 1\right), \quad \bar{s} = \frac{1}{\gamma}\left(e^{\gamma(1-\beta)\tau} - 1\right) \quad \text{at} \quad \alpha = 1, \tag{24}$$

showing that the mean size increases exponentially with time. On the other hand, the mean size becomes linear in time when $\gamma \to 0$, corresponding to the length-independent growth rate for NWs [35]:

$$\bar{s} = (1-\beta)\tau \quad \text{at } \gamma = 0. \tag{25}$$

It is easy to integrate Eq. (19) for the variance, giving

$$D(\bar{s}) = \frac{1+\beta}{1-\beta}\frac{1}{\gamma(1-2\alpha)}[1+\gamma\bar{s} - (1+\gamma\bar{s})^{2\alpha}], \ \alpha \neq 1/2, \tag{26}$$

$$D(\bar{s}) = \frac{1+\beta}{(1-\beta)\gamma}(1+\gamma\bar{s})\ln(1+\gamma\bar{s}), \quad \alpha = 1/2. \tag{27}$$

At $\beta = 0$, this is reduced to the result of Ref. [31] in the absence of evaporation. At $\gamma = 0$, we resume the result of Ref. [35] for self-catalyzed III–V NWs whose axial growth rate is driven by the direct impingement and evaporation of a group V element. As expected, enhanced evaporation always broadens the SD.

Figure 1 shows the variance versus mean size of Green's function at a fixed $\gamma = 0.1$, $\beta = 0.3$ and typical $\alpha = 0$, $1/3$, $1/2$, $2/3$, and 1, compared to the same systems in the absence of evaporation. As discussed in detail in Ref. [31], $\alpha = 0$ is the case of the adsorption-induced growth of NWs or surface islands growing on a two-dimensional (2D) substrate in the diffusion regime, $\alpha = 1/3$ corresponds to three-dimensional (3D) droplets fed from a 3D vapor in the diffusion regime or 3D Stranski-Krastanov islands growing from a metastable 2D wetting layer in the ballistic regime, $\alpha = 1/2$ is typical for 2D surface islands growing in the ballistic regime, $\alpha = 2/3$ corresponds to 3D droplets fed from a 3D vapor in the ballistic regime, and $\alpha = 1$ is the case of NWs growing by surface diffusion of adatoms. Poisson SD corresponds to the minimum width of the SD and is observed only when $\alpha = 0$ and $\beta = 0$, that is, at a size-independent growth rate $ds/d\tau = 1$ without evaporation. All other SDs in linear growth systems are broader than Poissonian, with the variance increasing toward larger growth index α and higher evaporation rate β.

We now consider the typical SD shapes in heterogeneous growth, where the nucleation rate can often be approximated by [31,32,34,35,37]

$$J(\tau) = be^{-b\tau}. \tag{28}$$

Here, $b = t_g/t_{\text{inc}}$ is the ratio of the characteristic growth time of large nanoparticles t_g over the incubation time t_{inc} required to attach the very first monomer to a nucleation seed, for example, to nucleate the very first nanowire monolayer from a catalyst droplet resting on a dissimilar substrate. Heterogeneous nucleation is difficult when $b \ll 1$. Following the general rule [31], the SD is given by

$$f(s,\tau) = \int_0^\tau d\tau' F(s,\tau')J(\tau-\tau'). \tag{29}$$

Using Eqs. (18) and (28) and repeating the procedure described in detail in Ref. [31], the SD is obtained in the form

$$f(s,\bar{s}) = \frac{b}{2(1-\beta)}\exp\left[\frac{b}{(1-\beta)}(s-\bar{s}) + \frac{b^2 D(\bar{s})}{2(1-\beta)^2}\right] \times \operatorname{erfc}\left[\frac{s-\bar{s}}{\sqrt{2D(\bar{s})}} + \frac{b}{1-\beta}\sqrt{\frac{D(\bar{s})}{2}}\right], \tag{30}$$

where $D(\bar{s})$ is defined in Eq. (26) or Eq. (27) for a given α and γ.

The mean size and variance of the fully formed SD such that $f(0,\bar{s}) = 0$ equal

$$\langle s\rangle = \bar{s} - \frac{1-\beta}{b}, \quad \sigma^2 = D + \left(\frac{1-\beta}{b}\right)^2. \tag{31}$$

Hence, the mean size of the SD decreases and its variance increases due to the nucleation delay at small $b \ll 1$. However, for any b we have the asymptotic relationship

$$\frac{\sigma^2}{\langle s\rangle} \to \frac{D(\bar{s})}{\bar{s}} \quad \text{at } \langle s\rangle \to \infty \tag{32}$$

showing that the ratio of the variance over mean size is determined by that of Green's function for large enough $\langle s\rangle$. The asymptotic relationship given by Eq. (32) applies for large enough sizes such that $\bar{s} \gg (1-\beta)/b$ and $D \gg (1-\beta)^2/b^2$, where the second condition is usually stronger than the first one. Of course, there is no guarantee that the asymmetry caused by the nucleation delay is completely forgotten in the experimental SD. This important question will be considered in Sec. VII. From Eqs. (26) and (27) it follows that

$$\begin{aligned}
&\frac{D(\bar{s})}{\bar{s}} \to \frac{1+\beta}{1-\beta}\frac{1}{1-2\alpha}, \quad \alpha < 1/2,\\
&\frac{D(\bar{s})}{\bar{s}} \to \frac{1+\beta}{1-\beta}\ln(\gamma\bar{s}), \quad \alpha = 1/2,\\
&\frac{D(\bar{s})}{\bar{s}} \to \frac{1+\beta}{1-\beta}\frac{1}{2\alpha-1}(\gamma\bar{s})^{2\alpha-1}, \quad \alpha > 1/2.
\end{aligned} \tag{33}$$

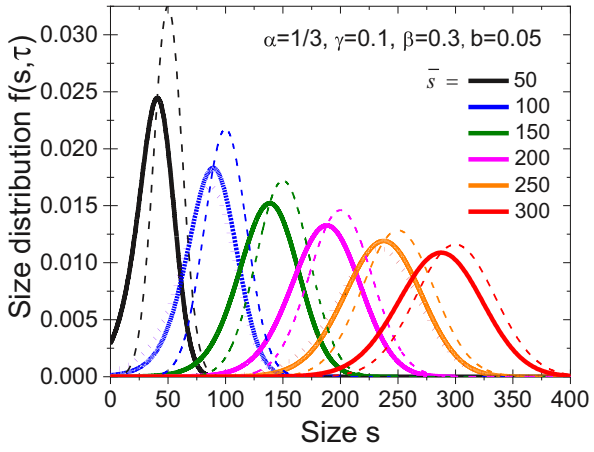

FIG. 2. Evolution of the SD $f(s,\bar{s}) = f[s,\bar{s}(\tau)]$ at $\alpha = 1/3$, $\gamma = 0.1$, $\beta = 0.3$, $b = 0.05$, and different $\bar{s}$ shown in the legend (full lines), compared to the corresponding Green function (dashed lines). It is seen that the SD is very asymmetric at the beginning due to the long nucleation delay at a small b. As the growth proceeds, the SD shape becomes symmetric and very similar to that of Green's function, with a constant shift becoming negligible at $\bar{s} \to \infty$. Symbols at $\bar{s} = 150$ and 250 show numerical solution to the continuum RE given by Eq. (2) for the same parameters.

The last expression is reduced to $D(\bar{s})/\bar{s} \to [(1+\beta)/(1-\beta)]\gamma\bar{s}$ at $\alpha = 1$. Therefore, the asymptotic SDs at $\alpha < 1/2$ are quasi-Poissonian, with the variance scaling linearly with the mean size. The threshold value of $\alpha = 1/2$ corresponds to only logarithmic spreading of the ratio $D(\bar{s})/\bar{s}$. At $\alpha > 1/2$, the ratio $D(\bar{s})/\bar{s}$ scales with the mean size as $(\gamma\bar{s})^{2\alpha-1}$. This yields the SD broadening which is much larger than Poissonian. For the size-linear growth rate, $D(\bar{s})/\bar{s}$ becomes proportional to $\bar{s}$, as in the case of Polya SD [28,31,33,34]. The effect of evaporation on the SD broadening is given by the same factor $(1+\beta)/(1-\beta)$ for any α, showing again that the SD becomes wider for higher evaporation rates. This result was obtained earlier at $\alpha = 0$ [35]. Overall, these results generalize the earlier ones [31] to linear systems with evaporation of material.

Figure 2 shows the evolution of $f(s,\bar{s})$ given by Eq. (30) at $\alpha = 1/3$, $\beta = 0.3$, $b = 0.05$ and different $\bar{s}$. The SD is asymmetric at the beginning, with a much longer tail toward smaller sizes due to the long nucleation delay at $b = 0.05$. However, it evolves to a symmetric Gaussian shape in the large time limit, with the variance becoming almost identical to the one of Green's function. This illustrates the property given by Eqs. (31) and (32), that is, negligible influence of the nucleation step on the SD shape for large enough sizes. Numerical solution to the initial continuum RE given by Eq. (2) with the same condensation-evaporation growth rates and the boundary condition corresponding to the nucleation rate defined in Eq. (28) is only slightly wider than the analytical one at $\bar{s} = 150$, and almost identical to the latter at $\bar{s} = 250$. This good quantitative correlation justifies the assumptions made in Sec. II.

Figure 3 shows how the SD shape changes with the growth index α at a fixed $\gamma = 0.1$, $\beta = 0.3$, $b = 0.05$, and $\bar{s} = 400$. As in Ref. [31], the SDs rapidly broaden with increasing α,

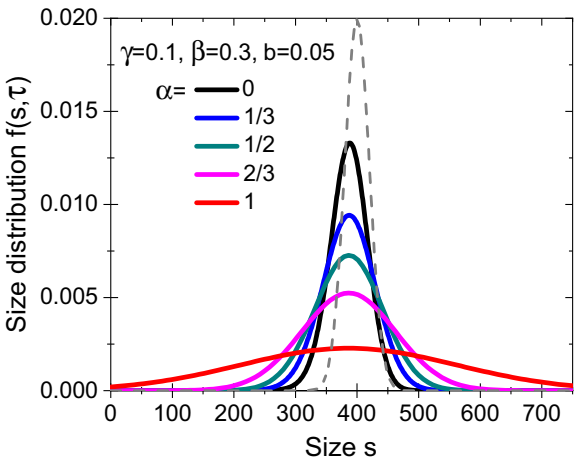

FIG. 3. SD shapes at a fixed $\bar{s} = 400$, $\gamma = 0.1$, $\beta = 0.3$, $b = 0.05$, and different α from 0 to 1 shown in the legend. The SDs rapidly broaden for larger α. All SDs are almost symmetrical and are wider than Poissonian, shown by the dashed line for the same $\bar{s}$.

demonstrating the huge effect of the growth index on the SD shape. At a fixed evaporation coefficient $\beta = 0.3$, all SDs are broader than Poissonian. The effect of nucleation delay is almost negligible at a large $\bar{s} = 400$, which is why the SDs are nearly symmetric around the mean size.

Figure 4 shows the effect of evaporation on the SDs at a fixed $\bar{s} = 1000$, $\alpha = 1$, $\gamma = 0.01$, and $b = 0.05$. These Polya SDs apply to the practical case of semiconductor NWs growing by surface diffusion of adatoms [33,34,43,44], with a nucleation delay and desorption or downward diffusion of material from a catalyst droplet. The role of desorption in this case has not been considered so far to our knowledge. The SDs are symmetrical and rapidly broaden for larger evaporation coefficients β, showing that the growth regimes with high desorption rates (occurring at a low supersaturation of the vapor phase) are undesirable for the length uniformity of vapor-liquid-solid NWs.

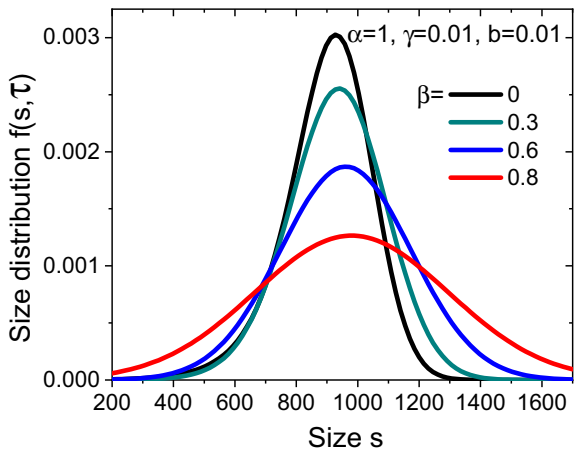

FIG. 4. SD shapes at a fixed $\bar{s} = 1000$, $\alpha = 1$, $\gamma = 0.01$, $b = 0.05$, and different β shown in the legend. It is seen that enhanced evaporation (desorption or downward diffusion for NWs) leads to a very significant broadening of the SDs toward larger β.

IV. CLASSICAL NUCLEATION THEORY IN OPEN SYSTEMS

We now consider homogeneous nucleation and growth of nanoparticles in systems with a restricted number of monomers which are used for growth and continuously added to a system via pumping using an external flux [1–8,12,17,21,22,27,29,30,42]. In this case, the condensation-evaporation rate constants for large enough s (which are much larger than the critical size of CNT [8,21]) are given by

$$W^+(s) = (\zeta + 1)s^\alpha, \quad W^-(s) = s^\alpha. \tag{34}$$

As above, we measure time τ in the units of a characteristic growth time t_g. The time dependent supersaturation $\zeta(\tau)$ is governed by the nanoparticle nucleation and growth and the material influx. Below we study only Green's function of the SD. This is relevant in the large time limit where the nucleation-induced variance [5,14,22] is almost negligible. On the other hand, we do not consider the late Ostwald ripening stage [45] which in many cases can be disabled by pumping [2,21]. For example, it is never observed in systems with a time-independent influx or deposition rate [2].

Our aim is calculating the variance of Green's function given by Eq. (19) with $W^+(s) - W^-(s) = \zeta s^\alpha$ and $W^+(s) + W^-(s) = (\zeta + 2)s^\alpha$, where ζ is a time-dependent function. This complicates the treatment with respect to a simpler case of linear growth systems studied in Sec. III. We note, however, that supersaturation tends to zero in the asymptotic growth stage [8] and hence the mean size is simply given by pumping

$$\bar{s} = k\tau^p. \tag{35}$$

Here, p is the pumping index which equals 1 in the most common case of a time-independent material influx and k is a certain coefficient which depends on the nanoparticle density [5,12,14,18,21,22] and the characteristic times of growth and pumping. For example, at $p = 1$ the material balance can be put in the form

$$\Omega(n_1 + N\bar{s}) = \frac{t}{t_\infty} + \Omega n_1^{\rm eq}, \tag{36}$$

where Ω is the elementary volume or surface area per monomer in the condensed phase, n_1 is the concentration of free monomers at time t, N is the number density of nanoparticles which is established in the nucleation stage and remains constant in the growth stage, t_∞ is the characteristic time of pumping, and $n_1^{\rm eq}$ is the equilibrium concentration of monomers in the mother phase. The left side gives the total number of monomers in the mother phase and in the islands, with the latter being reasonably approximated by the term $\Omega N\bar{s}$ for sufficiently narrow SDs whose variance remains much smaller than the mean size squared. Using the definition of supersaturation, $\zeta = n_1/n_1^{\rm eq} - 1$, and using $\zeta \to 0$ for long enough times, we get

$$\bar{s} \to \frac{1}{\Omega \mathrm{N}} \frac{t_g}{t_\infty} \frac{t}{t_g} = k\tau, \quad k = \frac{1}{\Omega \mathrm{N}} \frac{t_g}{t_\infty}. \tag{37}$$

Therefore, the coefficient k is inversely proportional to N and decreases for lower ratio t_g/t_∞. As discussed in detail in Refs. [18,22], one can tune the growth conditions to maximize the value of k, which suppresses the SD broadening in the kinetic growth stage.

Using Eq. (35) with arbitrary p, we obtain

$$\frac{d\bar{s}}{d\tau} = kp\tau^{p-1} = \zeta\bar{s}^\alpha. \tag{38}$$

This allows us to find supersaturation as a function of τ or $\bar{s}$ in the form

$$\zeta = pk^{1-\alpha}\tau^{(1-\alpha)p-1} = pk^{1/p}\bar{s}^{1-\alpha-1/p}. \tag{39}$$

Of course, the pumping index p must satisfy the condition of supersaturation decrease (or stabilization to a small constant) at a given α. Using

$$\begin{aligned} W^+(\bar{s}) - W^-(\bar{s}) &= pk^{1/p}\bar{s}^{1-1/p}, \\ W^+(\bar{s}) + W^-(\bar{s}) &= pk^{1/p}\bar{s}^{1-1/p} + 2\bar{s}^\alpha \end{aligned} \tag{40}$$

in Eq. (19) and integrating, we find the variance of the Gaussian Green function,

$$D(\bar{s}) = \frac{\bar{s}}{2/p - 1} + \frac{2}{pk^{1/p}} \frac{1}{\alpha + 3/p - 2}\bar{s}^{\alpha+1/p}. \tag{41}$$

Again, the pumping index must be such that both denominators in this expression are positive or zero, with the latter case corresponding to only logarithmic broadening of the SD [21].

For the ratio $D(\bar{s})/\bar{s}$, Eq. (41) yields

$$\frac{D(\bar{s})}{\bar{s}} \to \frac{1}{2/p - 1} + \frac{2}{pk^{1/p}} \frac{1}{\alpha + 3/p - 2}\bar{s}^{\alpha+1/p-1}, \tag{42}$$

which is reduced to

$$\frac{D(\bar{s})}{\bar{s}} \to 1 + \frac{2}{k(\alpha + 1)}\bar{s}^\alpha \tag{43}$$

at $p = 1$. As above, the asymptotic ratio of the SD $\sigma^2/\langle s\rangle$ equals $D(\bar{s})/\bar{s}$ due to a negligible contribution of the nucleation-induced broadening at $\bar{s} \to \infty$. According to Eq. (42), the SDs in CNT in open systems with pumping broaden for larger α and lower p, as shown in Fig. 5. Therefore, slower pumping always leads to wider SDs. In contrast to linear systems where the ratio $D(\bar{s})/\bar{s}$ remains constant at $\alpha < 1/2$ [see Eqs. (33)], the SDs in CNT with a time-independent influx (at $p = 1$) broaden wider than Poissonian for any $\alpha > 0$ as given by Eq. (43).

In the specific case of 3D droplets growing from supersaturated vapors in the ballistic regime ($\alpha = 2/3$), it was argued [12] that the SD maintains its time-independent double exponential shape in terms of the invariant size ρ, which for this system equals the dimensionless radius of the droplet. Spreading of the "invariant" SD at arbitrary α was later studied in Ref. [21], where the tendency for the suppression of spreading with increasing α was confirmed. This property is widely used in the growth modeling because the suppressed SD broadening allows for neglect of the second derivative with respect to size in the continuum RE [5,8,12,14,18]. Interestingly, however, Eqs. (42) or (43) show the monotonic increase of the SD broadening with α in terms of the number of monomers in the nanoparticle s. This feature also follows from the two known exactly solvable cases for linear systems

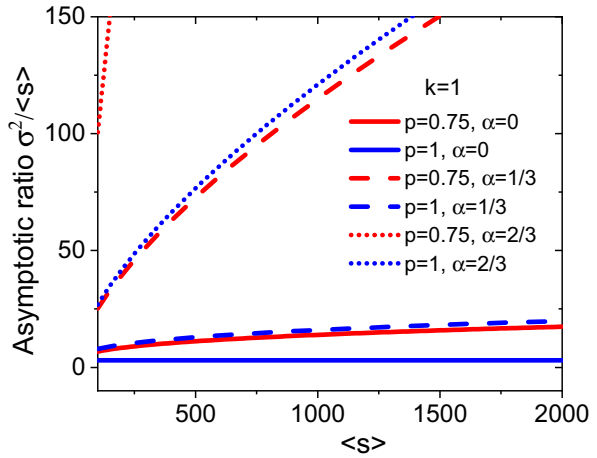

FIG. 5. Ratio $\sigma^2/\langle s\rangle$ vs mean size of the SDs in CNT in open systems with different pumping index p and growth index α shown in the legend. The variance increases with increasing α and decreasing p. Quasi-Poisson SD with a constant $\sigma^2/\langle s\rangle$ is observed only at $p = 1$ and $\alpha = 0$.

at $\alpha = 0$ [quasi-Poissonian SD with $D(\bar{s})/\bar{s} \to$ const [32,35]) and at $\alpha = 1$ (Polya-type SD with $D(\bar{s})/\bar{s} \propto \bar{s}$ [33,34]]. Consequently, both theoretical methods of the growth modeling of nanostructures and broadening of the real SDs largely depend on the choice of size variable. In the next section, we try to clarify the trends of the SD shapes in terms of s or ρ.

V. BROADENING IN TERMS OF NATURAL VERSUS INVARIANT VARIABLES

A. Linear growth systems

To find the relationship between the asymptotic Green functions of the continuum RE in terms of natural and invariant variables, we note that Eqs. (23) for large enough sizes are reduced to

$$s \to \gamma^{\alpha/(1-\alpha)}[(1-\beta)(1-\alpha)r]^{1/(1-\alpha)},$$
$$\bar{s} \to \gamma^{\alpha/(1-\alpha)}[(1-\beta)(1-\alpha)\tau]^{1/(1-\alpha)}, \quad \alpha < 1. \tag{44}$$

We insert this into Eq. (18) for Green's function with $D(\bar{s})$ given by the corresponding Eq. (33), present it in terms of r and τ according to Eq. (17), and use $(r^{1/(1-\alpha)} - \tau^{1/(1-\alpha)})^2 \cong \tau^{2\alpha/(1-\alpha)}(r-\tau)^2/(1-\alpha)^2$. This allows us to resume the Gaussian given by Eq. (10) with the asymptotic variance

$$\psi(\tau) \to \frac{1+\beta}{1-\beta}\frac{(1-\alpha)^2}{1-2\alpha}[(1-\beta)(1-\alpha)]^{-1/(1-\alpha)}\gamma^{-\alpha/(1-\alpha)} \times \tau^{(1-2\alpha)/(1-\alpha)}, \quad \alpha < 1/2,$$
$$\psi(\tau) \to 0, \quad \alpha > 1/2. \tag{45}$$

Thus, the "invariant" Green function $G(r,\tau)$ in linear systems broadens with τ at $\alpha < 1/2$ and becomes a delta function at $\alpha > 1/2$, with the threshold case of $\alpha = 1/2$ corresponding to logarithmic broadening. This result is fully consistent with Ref. [21] and supports the time invariance of the SD at $\alpha = 2/3$ introduced in Ref. [12]. According to Eq. (45), the invariant SDs are not affected by kinetic fluctuations for any $\alpha > 1/2$. In other words, they remain truly invariant in the kinetic growth stage, with the SD width being determined in the nucleation stage [5,12,14].

Comparison of broadening in different growth systems becomes clearer if presented in terms of the ratio of the variance over the mean size. For the ratio $\psi(\tau)/\tau$ introduced earlier, Eqs. (44) and (45) give

$$\frac{\psi(\tau)}{\tau} \to \frac{1+\beta}{1-\beta}(1-\beta)^{-1/(1-\alpha)}\gamma^{-\alpha/(1-\alpha)}\frac{(1-\alpha)^2}{1-2\alpha}\tau^{-\alpha/(1-\alpha)}, \quad \alpha < 1/2,$$
$$\frac{\psi(\tau)}{\tau} \to 0, \quad \alpha > 1/2. \tag{46}$$

Comparing this to Eqs. (33), one can see that at $\alpha < 1/2$, the natural ratio of variance versus mean size $D(\bar{s})/\bar{s}$ tends to a time-independent value which increases with α, while the invariant ratio $\psi(\tau)/\tau$ decreases with time and its decrease is faster for larger α. The only case where the two representations are equivalent is the Poisson growth at $\alpha = 0$. This is not surprising because the natural and invariant variables are identical. At $\alpha > 1/2$, the natural ratio $D(\bar{s})/\bar{s}$ increases with $\bar{s}$ and its increase is faster for larger α, while the invariant SD does not spread at all. Overall, the SD broadening in terms of the number of monomers in the nanoparticle s is enhanced for larger α, while it is suppressed in terms of the invariant variable r, as shown in Fig. 6(a).

B. Classical nucleation theory at $p = 1$

According to Eqs. (34), the regular growth rate in terms of the natural variable is given by $ds/d\tau = \zeta s^{\alpha}$. The invariant size of CNT is defined according to [12,14,21,22]

$$\frac{d\rho}{d\tau} = \zeta. \tag{47}$$

Therefore s and ρ are related by

$$s = [(1-\alpha)\rho]^{1/(1-\alpha)}, \quad \bar{s} = [(1-\alpha)z]^{1/(1-\alpha)}, \tag{48}$$

where we again assume that $\alpha < 1$. Using this in Eq. (18) together with Eq. (41) for $D(\bar{s})$ at $p = 1$ and repeating the above procedure for expressing the SD in terms of the invariant variables, we obtain the invariant Green function in the form of Gaussian [21]

$$G(\rho, z) = \frac{1}{\sqrt{2\pi\psi(z)}}\exp\left[-\frac{(\rho-z)^2}{2\psi(z)}\right]. \tag{49}$$

Here, the variance is given by

$$\psi(z) \to [(1-\alpha)z]^{(1-2\alpha)/(1-\alpha)} + \frac{2}{k}\frac{(1-\alpha)z}{1+\alpha}, \quad \alpha < 1/2,$$
$$\psi(z) \to \frac{2}{k}\frac{(1-\alpha)z}{1+\alpha}, \quad \alpha > 1/2. \tag{50}$$

The first term in Eq. (50) at $\alpha < 1/2$ is similar to the one in Eq. (45) for linear systems and describes quasi-Poissonian broadening of the SD. As above, it decreases with increasing α and disappears at $\alpha > 1/2$. The second term describes additional broadening in the asymptotic growth stage where supersaturation tends to zero [21]. At a time-independent influx ($p = 1$), it scales linearly with z, with a coefficient which

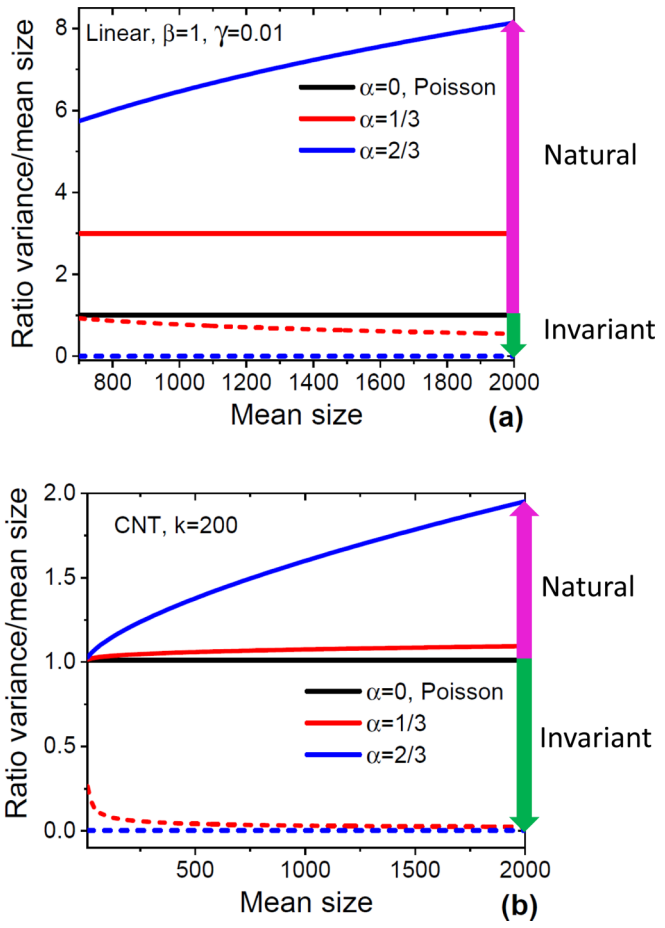

FIG. 6. Comparison of the asymptotic variance vs mean size in terms of natural or invariant variables for (a) linear growth systems and (b) CNT at $p = 1$ for three different α shown in the legend. Kinetic broadening of the natural SD increases with α, while broadening of the invariant SD decreases with α. The Poisson case is resumed only at $\alpha = 0$.

decreases for larger α. We remind that this additional broadening can be made rather small even for large enough sizes by optimizing the growth conditions to increase the value of k. However, this term dominates in the limit $z \to \infty$ for any $\alpha > 0$ and gives quasi-Poisson broadening with $\psi(z) \propto z$.

For the ratio $\psi(z)/z$, Eqs. (50) yield

$$\frac{\psi(z)}{z} \to (1-\alpha)^{(1-2\alpha)/(1-\alpha)} z^{-\alpha/(1-\alpha)} + \frac{2}{k}\frac{1-\alpha}{1+\alpha}, \quad \alpha < 1/2,$$
$$\frac{\psi(z)}{z} \to \frac{2}{k}\frac{1-\alpha}{1+\alpha}, \quad \alpha > 1/2. \tag{51}$$

Comparing this to Eq. (43), one can see that the natural ratio of variance versus mean size $D(\bar{s})/\bar{s}$ is always larger than unity (the Poisson case) and gradually increases with the growth index α, while the invariant ratio $\psi(z)/z$ is usually smaller than unity (this requires $k \gg 1$) and gradually decreases with α, as shown in Fig. 6(b). Kinetic broadening of the SDs in terms of the natural variable s increases for larger α for both linear growth systems and CNT. This trend is reversed for the SDs over the invariant variable r or ρ.

As a general conclusion, treatment of the SDs in terms of the invariant size indeed allows for minimization of the kinetic broadening, particularly for $\alpha > 1/2$. However, special care should be taken for the correct interpretation of the results. In particular, the invariant SDs become narrower for larger α, while the SDs over the number of monomers s becomes wider for larger α. For example, growth of 3D droplets from supersaturated vapors in the ballistic regime at $\alpha = 2/3$ [5,12,14,21] may yield a time-invariant and narrow SD over the droplet radii $r \propto s^{1/3}$, but the SD over s is very broad and rapidly spreads as the droplets grow. The growth regime should become diffusionlike for very large droplets ($\alpha = 1/3$) [8], in which case the SD may be time invariant for the surface area ($\rho \propto s^{2/3} \propto r^2$). The natural SD over s is affected by the kinetic broadening, but its spreading is less than in the ballistic regime at $\alpha = 2/3$. The same observation holds for the Stranski-Krastanov islands at $\alpha = 1/3$ [17,18]. The SD is narrow for the island surface area, which may be advantageous for surface-related effects such as adsorption, whereas the light emitting properties are governed by the number of semiconductor atoms or III–V pairs s [46] for which the SD is broad and spreads with time. III–V semiconductor NWs growing by surface diffusion of group III adatoms at $\alpha = 1$ ($ds/d\tau \to \gamma s$ at large s) [33,34] feature the broadest Polya-like SD over their lengths s, with $D(\bar{s}) \propto \gamma \bar{s}^2$. The SD becomes narrow and time invariant in terms of the logarithmic invariant variable $\rho = \gamma^{-1} \ln s$, which is meaningless.

VI. SIZE DISTRIBUTION OVER A GIVEN VARIABLE: INVARIANT OR NOT?

The invariant variable corresponds to a size-independent regular growth rate at a given growth index α and hence is fixed for a given growth law. Using the same approach as above, we can ask the question of whether the SD in terms of the variables

$$y = s^{1/m}, \quad \bar{y} = \bar{s}^{1/m} \tag{52}$$

is time invariant at a given α. The power index m equals 1, 2, or 3 in the typical cases, corresponding for example to the total number of monomers (or the volume) of a 3D nanoparticle with a fixed shape at $m = 1$, its surface area at $m = 2$, or linear size ("radius") at $m = 3$. We saw earlier that the time invariance or kinetic broadening of the SD is determined entirely by the variance of Green's function. We introduce Green's function of the continuum RE in terms of y by the general definition

$$H(y, \bar{y})dy = F(s, \bar{s})ds, \tag{53}$$

where the Gaussian $F(s, \bar{s})$ is given by Eq. (18). Using $ds/dy = my^{m-1}$ and

$$(s - \bar{s})^2 \cong m^2 \bar{y}^{2m-2}(y - \bar{y})^2, \tag{54}$$

we obtain

$$H(y, \bar{y}) = \frac{m\bar{y}^{m-1}}{\sqrt{2\pi D(\bar{y})}} \exp\left[-\frac{m^2 \bar{y}^{2m-2}}{2D(\bar{y})}\right]. \tag{55}$$

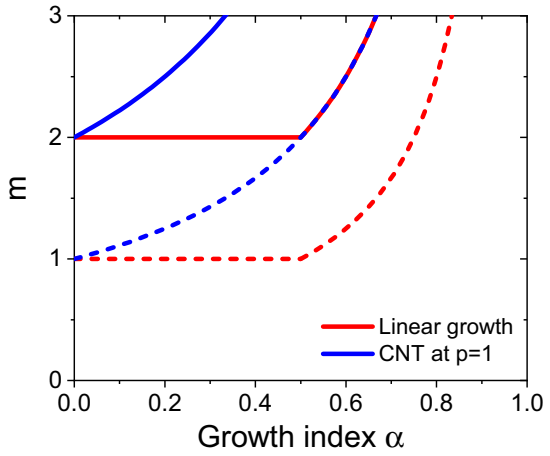

FIG. 7. Zones of time invariance (above the full curves) and broadening of the SDs (below the full curves) for linear growth systems and CNT at $p = 1$. The dashed lines correspond to quasi-Poisson broadening with $\psi(\bar{y}) \propto \bar{y}$. Any growth regimes below the dashed curves yield broadening which is larger than Poissonian.

This Green function is also Gaussian, with the variance

$$\psi(\bar{y}) = \frac{D(\bar{y})}{m^2 \bar{y}^{2m-2}}, \tag{56}$$

where D should be presented as a function of $\bar{y}$ using Eq. (52).

From Eqs. (33) for linear growth systems (at $\beta = 0$ and $\gamma = 1$), we get

$$\psi(\bar{y}) = \frac{1}{m^2(1-2\alpha)} \bar{y}^{2-m}, \quad \alpha < 1/2,$$
$$\psi(\bar{y}) = \frac{1}{m} \bar{y}^{2(1-m)} ln\bar{y}, \quad \alpha = 1/2,$$
$$\psi(\bar{y}) = \frac{1}{m^2(2\alpha-1)} \bar{y}^{2(m\alpha-m+1)}, \quad \alpha > 1/2. \tag{57}$$

From Eq. (43) for CNT at $p = 1$, we obtain

$$\psi(\bar{y}) = \frac{1}{m^2}\left[\bar{y}^{2-m} + \frac{2}{k(\alpha+1)} \bar{y}^{2-m+m\alpha}\right]. \tag{58}$$

Clearly, the time invariant SDs are observed when $\psi(\bar{y}) \to 0$ at large $\bar{y}$. This condition determines the critical index m_c above which the SDs over y are invariant at a given α. For linear growth systems, the condition for the time invariance is given by

$$m > m_c = \begin{matrix} 2 \text{ at } \alpha < 1/2, \\ 1/(1-\alpha) \text{ at } \alpha > 1/2. \end{matrix} \tag{59}$$

For CNT at $p = 1$, the same condition becomes

$$m > m_c = 2/(1-\alpha), \tag{60}$$

and applies uniformly for any α.

These critical curves are shown in Fig. 7 in the form of $m(\alpha)$ diagrams, along with the curves corresponding to quasi-Poisson broadening of the SDs with $\psi(\bar{y}) \propto \bar{y}$. All geometrical characteristics of a nanoparticle lying above the critical curves are not influenced by kinetic fluctuations and their SDs are expected to be more homogeneous and time invariant. The SDs broaden below the critical curves, and they broaden faster than Poissonian below the dashed curves. The time-invariant zone is narrower in CNT than in linear growth systems due to additional broadening at zero supersaturation. We remind that the SDs in CNT at $p = 1$ do not undergo the Ostwald ripening, which is why the time invariant shape will be maintained forever. Figure 7 shows, for example, that the SD over the nanoparticle radii in the 3D case ($m = 3$) remains invariant for any $\alpha < 2/3$ in linear growth systems and for any $\alpha < 1/3$ in CNT. On the other hand, the SD over the nanoparticle volume ($m = 3$) can only be quasi-Poissonian in linear growth and is broader than Poissonian for any $\alpha > 0$ in CNT. The invariant zones narrow up with increasing the growth index α in both cases, which is why the growth regimes with lower α are always favorable for the size homogeneity.

VII. THEORY AND EXPERIMENT

We now consider particular growth systems for which the regular growth rater is either independent of s or scales linearly with s for large enough s. We will compare the variance versus mean size for the experimental SDs or those obtained using kinetic Monte Carlo (KMC) simulations in terms of the ratio $\sigma^2/\langle s \rangle$ taking into account (i) Poissonian broadening, (ii) additional kinetic broadening due to surface diffusion, (iii) evaporation of material, and (iv) nucleation delay for asymmetric SDs. Using Eq. (26) for $D(\bar{s})$ at $\alpha = 1$, we have

$$D(\bar{s}) = \frac{1+\beta}{1-\beta}(\bar{s} + \gamma \bar{s}^2), \tag{61}$$

which is reduced to $D(\bar{s}) = [(1+\beta)/(1-\beta)]\bar{s}$ for systems with s-independent growth rates (at $\gamma = 0$). From Eqs. (31), the ratio $\sigma^2/\langle s \rangle$ can be presented solely as a function of $\langle s \rangle$:

$$\frac{\sigma^2}{\langle s \rangle} = \frac{[(1-\beta)/b]^2[1+\gamma(1+\beta)/(1-\beta)] + (1+\beta)/b}{\langle s \rangle} + \frac{1+\beta}{1-\beta} + 2\gamma\frac{(1+\beta)}{b} + \frac{1+\beta}{1-\beta}\gamma\langle s \rangle. \tag{62}$$

This expression contains three parameters γ, β, and b describing the effects of surface diffusion, evaporation, and nucleation delay, respectively. The Poissonian broadening in the absence of the three other effects (at $\gamma = \beta = 0$ and $b = 1$) corresponds to the minimum $\sigma^2/\langle s \rangle = 1$ for $\langle s \rangle \gg 1$. Clearly, the first term of Eq. (62) always tends to zero at large enough $\langle s \rangle$, showing that the effect of nucleation delay on the SD shape dissapears provided that $\gamma = 0$. The second, $\langle s \rangle$-independent term gives a constant ratio $\sigma^2/\langle s \rangle = (1+\beta)/(1-\beta)$ for Poissonian growth with evaporation. This ratio can be very large when β is close to unity. The third term is also $\langle s \rangle$ independent and describes additional broadening of the SDs in systems with surface diffusion ($\gamma > 0$) and nucleaton delay ($b \ll 1$). Finally, the last term is proportional to $\gamma\langle s \rangle$ and gives the Polya-type broadening of the SDs due to surface diffusion.

Figure 8 shows the ratios $\sigma^2/\langle s \rangle$ for different mean sizes and in different systems. In two systems, we clearly observe the linear scaling of $\sigma^2/\langle s \rangle$ with $\langle s \rangle$. Two-dimensional (2D) surface islands of different shapes (fractal or compact) studied by KMC in Ref. [23] grew at a high ratio of the surface diffusion coefficient over the deposition rate and without

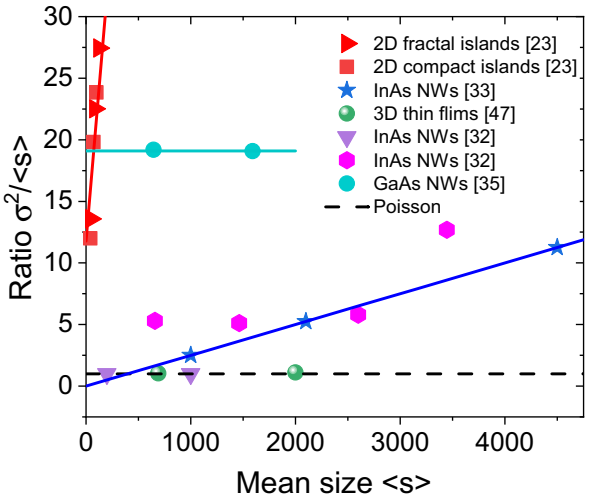

FIG. 8. The ratios $\sigma^2/\langle s\rangle$ obtained by KMC simulations for 2D fractal and compact islands in the precoalescence stage of their growth for the surface coverages of 0.05, 0.1, and 0.15 [23]; for Au-catalyzed InAs NWs whose growth is driven by surface diffusion of In adatoms [33]; for surface profiles of 3D thin films at low temperatures [47]; for Au-catalyzed InAs NWs grown without surface diffusion of In adatoms from thermally dewetted Au films or Au colloidal nanoparticles [32]; and for Ga-catalyzed GaAs NWs [35]. The lines show the fits obtained from Eq. (62) with the parameters summarized in Table I. The dashed line corresponds to the minimum Poisson broadening at $\sigma^2/\langle s\rangle = 1$. The data points without the line are fitted with the four different b values given in Table I. The maximum broadening of the SDs is observed for 2D islands, where the ratio $\sigma^2/\langle s\rangle$ scales linearly with $\langle s\rangle$. InAs NWs growing by surface diffusion also show the linearly increasing $\sigma^2/\langle s\rangle$. However, it remains smaller than the ones for "quasi-Poissonian" InAs NWs or Ga-catalyzed GaAs NWs whose SDs broaden due to very long nucleation delay or high desorption rate of As atoms, respectively. The true Poissonian case of $\sigma^2/\langle s\rangle = 1$ is observed in only two cases.

evaporation ($\beta = 0$). Their nucleation is homogeneous and the nucleation rate may be more complex than the simple exponential decay given by Eq. (28). Furthermore, the coalescence may occur before the adatom density tends to zero and the SDs obtained in Ref. [23] do not tend to zero at $s = 0$. Therefore, Eq. (62) can be used only in the first approximation. Despite of this, the growth has a marked Polya-like character, with $\sigma^2/\langle s\rangle$ increasing linearly with $\langle s\rangle$. Based on our results, one may conclude that the growth rate of such islands is linear in s for large enough s, the property explained earlier by a competition of the growing islands for the diffusion flux from the substrate [3,6,7,23,28]. Due to the pronounced asymmetry of the SDs obtained in Ref. [23], we fit the corresponding ratios $\sigma^2/\langle s\rangle$ with $\gamma = 0.1$ and a small b of 0.017, as given in Table I. Au-catalyzed InAs NWs of Ref. [33] were grown at 450 °C under group V rich conditions. The vapor-liquid-solid growth is driven by surface diffusion of adatoms collected from the entire NW length, as explained in Sec. III. In adatoms are not expected to desorb at 450 °C. The measured SDs were perfectly symmetric [33], meaning that the effect of slow nucleation is negligible. Therefore, these SDs are fitted with $\beta = 0$, $b = 1$, and $\gamma = 0.0025$. The broadening of the SDs is much smaller than for 2D islands mainly due to a much smaller γ (0.0025 against 0.1).

TABLE I. Fitting parameters for different SDs shown in Fig. 8.

System	γ	β	b
2D surface islands [23]	0.1	0	0.017
Au-catalyzed InAs NWs growing by surface diffusion [33]	0.0025	0	1
Au-catalyzed InAs NWs growing with long nucleation delay [32]	0	0	0.005
			0.009
			0.013
			0.017
Ga-catalyzed GaAs NWs growing with high As desorption rates [35]	0	0.9	0.02
Poissonian InAs NWs [32]	0	0	1
Poissonian 3D thin films [47]	0	0	1

Au-catalyzed InAs NWs of Ref. [32] were grown using thermal dewetting of a thin Au film or Au colloids, where the latter appeared buried deep into the substrate in the annealing pregrowth step. This burial caused a long nucleation delay. The measured SDs were fully formed; however, they showed very long tails toward the smaller lengths. The four data points shown in Fig. 8 were perfectly fitted but with different b for each sample [32], summarized in Table I. The growth was quasi-Poissonian, without surface diffusion of In adatoms and at a low surface temperature of 380 °C. Therefore, the other fitting parameters are chosen at $\gamma = \beta = 0$. The large broadening effect in these NW SDs is entirely due to the long nucleation delay, and is comparable to that in the ensembles of InAs NWs growing by surface diffusion. When the nucleation effect is removed, as in InAs NWs of Ref. [32] grown from thermally dewetted Au films, the SDs become Poissonian. The Poisson SD is also observed in KMC simulations of three-dimensional (3D) homoepitaxial thin films grown at low temperatures in the absence of re-evaporation and surface diffusion ($\gamma = \beta = 0$, $b = 1$) [47]. In this case, the SD gives the probability to observe the random point of the film surface at a height of s monolayers from the substrate, and obey the set of Poissonian REs [47].

The broadest NW SDs are observed for Ga-catalyzed GaAs NWs grown at 635 °C on processed Si substrates [35]. Ga-catalyzed vapor-liquid-solid growth is always controlled by the kinetics of As atoms (in the excess of liquid Ga in the droplet) which are not diffusive ($\gamma = 0$) but desorb from the droplet due to the known high volatility. Therefore, the corresponding SDs are well fitted with $\beta = 0.9$, showing that about 90% of As arriving onto the droplet surface re-evaporates. The influence of the nucleation delay at $b = 0.02$, necessary to describe the initial asymmetry of the SDs for smaller lengths, becomes negligible at $\langle s\rangle > 600$.

The above comparison of different growth systems shows the following trends. The ratio $\sigma^2/\langle s\rangle$ scales linearly with $\langle s\rangle$ in systems where the growth rate is linear in s, and should become asymptotically larger than in any other system. However, this scaling largely depends on the value of γ and other

effects such as a limited diffusion length of group III adatoms on the NW sidewalls [33] or coalescence of 2D islands into continuum layers. Therefore, the real ratios $\sigma^2/\langle s\rangle$ may be smaller than in quasi-Poissonian systems with high evaporation rates or nucleation delays. If the regular growth rate is independent of s, the effect of evaporation is asymptotically larger than that of the nucleation delay, and remains forever in the measured SDs. The true Poisson SDs are rarely observed and seem to be the best case regarding the size uniformity within the ensembles of different nanoobjects. The only effect which can narrow the SDs below the Poisson limit is the nucleation antibunching, occurring due to a limited amount of material in a nanophase [36–38]. This effect was considered earlier only in the case without surface diffusion or evaporation [38]. Including these effects in the existing theory is far from obvious.

VIII. CONCLUSIONS

In conclusion, we summarize the main findings. First, an analytic approach of Ref. [31] has been generalized to include evaporation of material from a nanoparticle. In the case of heterogeneous nucleation and growth at a time-independent supersaturation, an analytic SD over the natural variable s has been obtained as given by Eq. (30). This SD depends on the four parameters—the growth index α, the evaporation coefficient β, the nucleation delay b and the diffusion parameter γ—and can reproduce very different shapes under different growth conditions. Evaporation has been shown to always increase the SD width. Second, CNT in open systems with pumping has been considered, where a similar approach allowed us to obtain an analytic Green function for the SDs over s. Third, it has been shown that the SDs in terms of the natural versus invariant variables show the opposite broadening trends, namely, the natural SDs broaden with increasing α, while the invariant SDs narrow with increasing α. Fourth, the zones of time invariance or broadening at different rates have been established for different size-dependent variables versus the growth index. Several growth systems have been considered from the viewpoint of the obtained results, including 3D thin films, 2D surface islands, and III–V semiconductor nanowires. These results should enable fine tuning of the growth conditions to narrow the SDs in terms of the required geometrical parameter such as the volume, surface area, linear size, or length of a nanostructure.

ACKNOWLEDGMENT

This work was supported by the Russian Science Foundation under Grant No. 19-72-30004.

[1] A. Venables, G. D. T. Spiller, and M. Hanbucken, Rep. Prog. Phys. **47**, 399 (1984).
[2] S. A. Kukushkin and A. V. Osipov, Prog. Surf. Sci. **51**, 1 (1996).
[3] H. Brune, Surf. Sci. Rep. **31**, 121 (1998).
[4] D. Kashchiev, *Nucleation: Basic Theory with Applications* (Butterworth-Heinemann, Oxford, 2000).
[5] F. M. Kuni, A. K. Shchekin, and A. P. Grinin, Phys. Usp. **171**, 345 (2001).
[6] J. W. Evans, P. A. Thiel, and M. C. Bartelt, Surf. Sci. Rep. **61**, 1 (2006).
[7] M. Einax, W. Dieterich, and P. Maass, Rev. Mod. Phys. **85**, 921 (2013).
[8] V. G. Dubrovskii, *Nucleation Theory and Growth of Nanostructures* (Springer, Heidelberg, 2014).
[9] E. W. Montroll and K. E. Shuler, J. Chem. Phys. **26**, 454 (1957).
[10] R. Glauber, J. Math. Phys. **4**, 294 (1963).
[11] C. C. Rankin and J. C. Light, J. Chem. Phys. **46**, 1305 (1967).
[12] F. M. Kuni and A. P. Grinin, Colloid J. USSR **6**, 412 (1984).
[13] T. Vicsek and F. Family, Phys. Rev. Lett. **52**, 1669 (1984).
[14] A. P. Grinin, V. B. Kurasov, and F. M. Kuni, Colloid J. USSR **52**, 371 (1990).
[15] P. A. Mulheran and J. A. Blackman, Philos. Mag. Lett. **72**, 55 (1995).
[16] D. D. Vvedensky, Phys. Rev. B **62**, 15435 (2000).
[17] A. V. Osipov, S. A. Kukushkin, F. Schmitt, and P. Hess, Phys. Rev. B **64**, 205421 (2001).
[18] V. G. Dubrovskii, G. E. Cirlin, and V. M. Ustinov, Phys. Rev. B **68**, 075409 (2003).
[19] T. Lummen and T. Kraska, J. Aerosol Sci. **36**, 1409 (2005).
[20] V. Holten and M. E. H. van Dongen, J. Chem. Phys. **130**, 014102 (2009).
[21] V. G. Dubrovskii, J. Chem. Phys. **131**, 164514 (2009).
[22] V. G. Dubrovskii and M. V. Nazarenko, J. Chem. Phys. **132**, 114507 (2010).
[23] M. Korner, M. Einax, and P. Maass, Phys. Rev. B **86**, 085403 (2012).
[24] J. Tersoff, C. Teichert, and M. G. Lagally, Phys. Rev. Lett. **76**, 1675 (1996).
[25] J. Jedrak, Phys. Rev. E **87**, 022132 (2013).
[26] V. A. Shchukin, N. N. Ledentsov, P. S. Kop'ev, and D. Bimberg, Phys. Rev. Lett. **75**, 2968 (1995).
[27] V. G. Dubrovskii and N. V. Sibirev, Phys. Rev. B **89**, 054305 (2014).
[28] V. G. Dubrovskii and N. V. Sibirev, Phys. Rev. E **91**, 042408 (2015).
[29] I. A. Babintsev, L. Ts. Adzhemyan, and A. K. Shchekin, Physica A **479**, 551 (2017).
[30] A. K. Shchekin, K. Koga, and N. A. Volkov, J. Chem. Phys. **151**, 244903 (2019).
[31] V. G. Dubrovskii, Phys. Rev. E **99**, 012105 (2019).
[32] V. G. Dubrovskii, N. V. Sibirev, Y. Berdnikov, U. P. Gomes, D. Ercolani, V. Zannier, and L. Sorba, Nanotechnology **27**, 375602 (2016).
[33] V. G. Dubrovskii, Y. Berdnikov, J. Schmidtbauer, M. Borg, K. Storm, K. Deppert, and J. Johansson, Cryst. Growth Des. **16**, 2167 (2016).
[34] V. G. Dubrovskii, J. Cryst. Growth **463**, 139 (2017).
[35] V. G. Dubrovskii, J. Barcus, W. Kim, J. Vukajlovic-Plestina, and A. Fontcuberta Morral, Nanotechnology **30**, 475604 (2019).

[36] F. Glas, J. C. Harmand, and G. Patriarche, Phys. Rev. Lett. **104**, 135501 (2010).

[37] F. Glas and V. G. Dubrovskii, Phys. Rev. Materials **1**, 036003 (2017).

[38] E. Koivusalo, T. Hakkarainen, M. D. Guina, and V. G. Dubrovskii, Nano Lett. **17**, 5350 (2017).

[39] J. W. P. Schmelzer and A. S. Abyzov, J. Chem. Phys. **134**, 054511 (2011).

[40] V. G. Dubrovskii, T. Xu, A. Dıaz Alvarez, S. R. Plissard, P. Caroff, F. Glas, and B. Grandidier, Nano Lett. **15**, 5580 (2015).

[41] J. Tersoff, Nano Lett. **15**, 6609 (2015).

[42] V. A. Shneidman, Phys. Rev. Lett. **101**, 205702 (2008).

[43] J. Johansson and M. H. Magnusson, M. H. J. Cryst. Growth **525**, 125192 (2019).

[44] V. G. Dubrovskii, H. Hijazi, N. I. Goktas, and R. R. LaPierre, J. Phys. Chem. C **124**, 17299 (2020).

[45] I. M. Lifshitz and V. V. Slezov, J. Phys. Chem. Solids **19**, 35 (1961).

[46] D. Bimberg, M. Grundmann, and N. N. Ledentsov, *Quantum Dot Heterostructures* (Wiley, New York, 1999).

[47] V. G. Dubrovskii and G. E. Cirlin, Tech. Phys. **42**, 1365 (1997).